



# The Mass-loss History of the Red Hypergiant VY CMa\*

Roberta M. Humphreys<sup>1</sup>, Kris Davidson<sup>1</sup>, A. M. S. Richards<sup>2</sup>, L. M. Ziurys<sup>3</sup>, Terry J. Jones<sup>1</sup>, and Kazunori Ishibashi<sup>4</sup>

<sup>1</sup>Minnesota Institute for Astrophysics, University of Minnesota, Minneapolis, MN 55455, USA; [roberta@umn.edu](mailto:roberta@umn.edu)

<sup>2</sup>Jodrell Bank, Department of Physics and Astronomy, University of Manchester, UK

<sup>3</sup>Departments of Astronomy and Chemistry, University of Arizona, USA

<sup>4</sup>Graduate School of Science, Nagoya University, Nagoya, 464-8602, Japan

Received 2020 November 19; revised 2020 December 11; accepted 2020 December 11; published 2021 February 4

## Abstract

Imaging and spectroscopy of the knots, clumps, and extended arcs in the complex ejecta of VY CMa confirm a record of high mass-loss events over the past few hundred years. Hubble Space Telescope/Space Telescope Imaging Spectrograph spectroscopy of numerous small knots close to the star allow us to measure their radial velocities from the strong KI emission and determine their separate motions, spatial orientations, and time since ejecta. Their ages concentrate around 70, 120, 200, and 250 yr ago. A KI emission knot only 50 mas from the star ejected as recently as 1985–1995 may coincide with an H<sub>2</sub>O maser. Comparison with VY CMa’s historic light curve from 1800 to the present shows several knots with ejection times that correspond with extended periods of variability and deep minima. The similarity of this correspondence in VY CMa with the remarkable recent dimming of Betelgeuse and an outflow of gas is apparent. The evidence for similar outflows from the surface of a more typical red supergiant suggests that discrete ejections are more common and surface or convective activity is a major source of mass loss for red supergiants.

*Unified Astronomy Thesaurus concepts:* [Circumstellar matter \(241\)](#); [Massive stars \(732\)](#); [Red supergiant stars \(1375\)](#); [Stellar mass loss \(1613\)](#)

## 1. Introduction

The famous red hypergiant VY CMa is one of a small class of evolved massive stars that represent a short-lived evolutionary phase characterized by extensive circumstellar ejecta, asymmetric ejections, and multiple high mass-loss events. VY CMa is an extreme case even among the rare hypergiant stars. The three-dimensional morphology of its complex circumstellar ejecta (Humphreys et al. 2007; Jones et al. 2007) and the massive, dusty condensations revealed by ALMA submillimeter observations (O’Gorman et al. 2015; Vlemmings et al. 2017; Kaminski 2019; Asaki et al. 2020) confirm a record of numerous high mass-loss events over the past few hundred years driven by localized, large-scale instabilities on its surface. VY CMa is one of the most important examples for understanding episodic mass loss and the role of possible surface activity and magnetic fields.

Ground-based optical spectroscopy of the central star and ejecta has been limited to 0.8 spatial resolution (Humphreys et al. 2005). Several small dusty knots and filaments within 1 arcsecond of the star very likely represent the most recent mass-loss events. We therefore obtained Hubble Space Telescope (HST)/Space Telescope Imaging Spectrograph (STIS) observations to probe VY CMa’s innermost ejecta and numerous small, diffuse condensations to the south and southwest of the star.

Our spectra of the small knots and filaments closest to the central star yielded a surprising result reported in Humphreys et al. (2019, hereafter Paper I). Very strong KI emission lines formed by resonant scattering (Humphreys et al. 2005) and the TiO and VO molecular spectra, long assumed to form in a dusty circumstellar shell, actually originate in a few small

clumps, a few 100 au from the star. Based on their motions, we found that they were ejected about 100 years ago and very likely represent VY CMa’s most recent active period. The KI lines are 10–20 times stronger in these nearest ejecta than on the star itself. The excitation of these strong atomic and molecular features present in the small knots therefore present an astrophysical problem. We showed that the clumps must have a nearly clear line of sight to the star’s radiation implying major gaps or holes in the circumstellar medium perhaps formed by large-scale activity.

In this second paper, we focus on the spectra of the knots and clumps visible in the images to the south and southwest of the star, the S knots, SW knots, and the SW clump (Humphreys et al. 2005, 2007). In the next section we describe our HST/STIS observations followed by a brief discussion of the spectrum of the central star and the presence of a small emission knot very close to the star possibly associated with H<sub>2</sub>O maser emission. In Section 4, the numerous KI emission peaks along the slits, their identification with the diffuse knots, their ejection ages, and the geometry of the SW clump are discussed. In the final section we summarize the recent mass-loss history of VY CMa. We find that numerous ejections over the past 200 years correspond to extended periods of major dimming in VY CMa’s light curve reminiscent of Betelgeuse’s recent unexpected behavior.

## 2. HST/STIS Observations

The HST/STIS observations were planned in two visits to allow two different slit orientations sampling the small knots and filaments immediately to the west and east of the star with three slit positions (Paper I), and to separate the individual knots to the south and southwest of the star with three slit positions as shown in Figure 1. The central star was observed in each visit.

\* Based on observations made with the NASA/ESA Hubble Space Telescope which is operated by the Association of Universities for Research in Astronomy, Inc., under NASA contract NAS 5-26555.

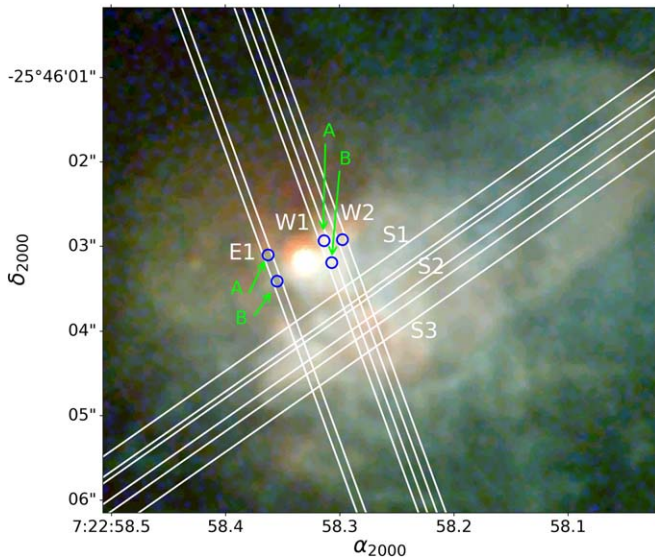


**Figure 1.** Composite image of VY CMA from Paper I showing positions of the slits and knots close to the star discussed in that paper.

We used the STIS/CCD with the G750M grating at tilts 7795 and 8561, with respective spectral resolutions of 6900 and 7600, to measure the K I emission doublet and the near-infrared Ca II absorption triplet and other absorption lines in the 8500 Å region. The K I lines, formed by resonant scattering, are the strongest emission features in VY CMA and are the best tracers of the gas. The strong Ca II lines however are reflected by dust, and are both redshifted and broadened by the dust scattering. The  $52 \times 0.1$  slit was used for the small knots and filaments to the west and east of the star. The  $0''.2$  slit width was chosen for the knots south of the star, discussed here, to enclose their somewhat more diffuse, extended structures and to account for their motions measured previously (Humphreys et al. 2007). These HST/STIS observations were completed on 2018 January 5 and February 11.

At  $\lambda \approx 7000$  Å, the basic spectral resolution of STIS is slightly better than  $0''.1$  (FWHM of the point-spread function, PSF). Since this is only about 2 CCD pixels we use the subpixel modeling technique developed for the Eta Car Treasury programs (Davidson 2006) to assure a consistent data PSF and to take full advantage of the HST’s spatial resolution along the slit. Consequently, the sampling scale in the processed spectra is  $0''.0253$  per pixel, rather than the CCD’s  $0''.05$  scale. Contemporary flat-field images were also obtained to correct for fringing in the red and were processed in the same way as the science images and normalized to be used as contemporary fringe flat-field images.

The different velocities measured in the spectrum of VY CMA are discussed in Humphreys et al. (2005). It is well established that the absorption and emission line velocities deviate from the systemic velocity inferred from the masers. As in previous papers, we adopt the emission velocity of VY CMA as our reference frame. The velocity of the K I emission measured in the  $0''.1$  slit,  $55 \text{ km s}^{-1}$  (Table 1), differs from that used in our 2005 and 2007 papers due to strong K I emission from compact knots in the wider slit in the ground-based spectra (see Paper I). In addition to the redshift and broadening due to scattering by dust, the absorption lines are also affected by the moving mirror effect.

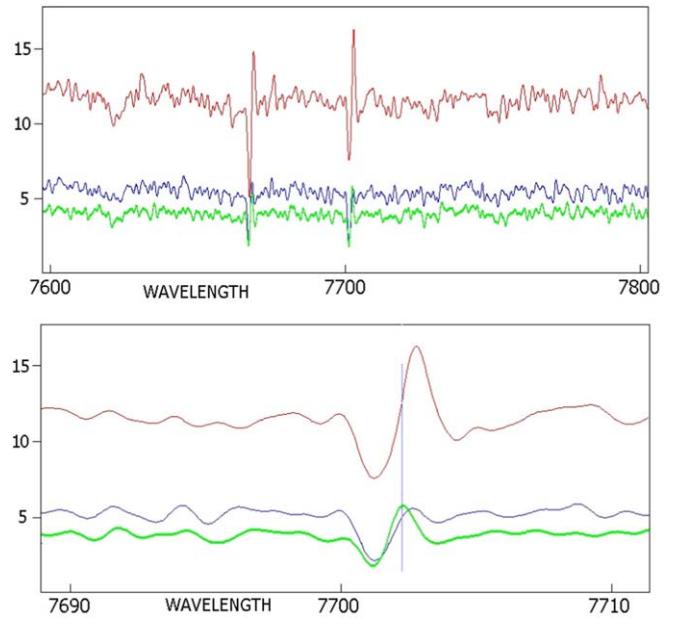


**Figure 2.** Upper: spectra of the K I lines on the star in the  $0''.1$  slit in blue and the  $0''.2$  slit in red. The K I lines from the small emission knot in the narrow slit just to the southwest of the star are shown in green. Lower: a close-up of the  $\lambda$  7701 K I profile. The vertical line marks the velocity of the inner knot just to the southwest of the star. The flux calibrated spectra are in units of  $10^{-14} \text{ W cm}^{-2} \text{ \AA}^{-1}$  vs. the vacuum wavelength in Å.

**Table 1**  
Heliocentric Velocities of the Star and Inner Knot

Object Slit	Avg. K I Em. Velocity ( $\text{km s}^{-1}$ )	K I Abs. Velocity ( $\text{km s}^{-1}$ )	Avg. Abs. Lines Velocity ( $\text{km s}^{-1}$ )
Star $0''.1$	$55 \pm 4$	7.0	$67.1 \pm 11$ (21)
Star $0''.2$	$68.7 \pm 4$	10.7	$60.7 \pm 11$ (18)
Inner knot $0''.1$	$47.6 \pm 2$	4.3	$65.7 \pm 8.4$ (19)

### 3. The Central Star

With the two different slit widths as well as their separate orientations, we have two sample sizes of the central star’s wind and innermost ejecta. The  $0''.1$  and  $0''.2$  slit widths correspond to  $\approx 120$  and  $240$  au, respectively, at the 1.2 kpc distance of VY CMA (Zhang et al. 2012). The dust formation zone of VY CMA is expected at about 100 au (Humphreys et al. 2005). The star’s spectrum with the  $0''.2$  slit therefore samples more of the dusty ejecta closest to the star. Its spectrum of the K I region is shown in Figure 2, together with the spectrum from the same spectral region obtained with the  $0''.1$  slit. The same width was used for the extractions. Stronger K I emission and also weak molecular emission is beginning to appear in the spectrum with the wider slit width. For example, the two weak emission features are due to TiO (Paper I). The K I emission lines from the wider slit also show a small shift to somewhat longer wavelengths due to the resonant scattering. The absorption lines, including the Ca II triplet plus lines of Fe I and Ti I, do not show a similar redshift relative to the narrower slit. Since these lines are seen via scattered light, the lack of any relative motion suggests very little expansion of the dusty inner ejecta. The radial velocities measured on the star with the two slits are summarized in Table 1.

The narrow  $0''.1$  slit also revealed a K I emission peak separated only 2 pixels or  $0''.05$  from the center of the star's spectrum. Given the slit's orientation on the star with PA  $20^\circ$ , this feature would be located just to its south–southwest. It is very likely a small knot of nebulosity or ejecta, the closest to the star. The K I spectrum of this inner knot is also shown in Figure 2. Its K I emission peaks have an average velocity of  $47.6 \text{ km s}^{-1}$ , slightly blueshifted by  $-7 \text{ km s}^{-1}$  relative to the star's K I velocity (Table 1), and similar to the velocities measured for the small knots to the west and east of the star in Paper I. It is too close to the star to be visible in any of the HST images (Humphreys et al. 2007). We therefore do not have a measured proper motion for it and its transverse velocity is not known. Its negative radial component implies that it is in front of the plane of the sky. Its distance corresponds to only 60 au from the star, within the star's dusty envelope. If we assume that its total velocity is similar to those for the knots just to the west of the star in Paper I ( $20\text{--}30 \text{ km s}^{-1}$ ), then this knot was ejected only  $\approx 10\text{--}15$  yr before our first epoch 1999 images, i.e., in 1985–1990.

There is an interesting possible correlation of this inner knot with  $\text{H}_2\text{O}$  maser emission peaks within 100 mas shown in Figure 17 in Asaki et al. (2020). Most are located to the south of the star. The figure shows a velocity data cube with local standard of rest (kinematic; LSRK) radial velocities. Our velocities are heliocentric. When corrected to the local standard of rest (LSR), the K I emission velocity of the inner knot is  $31.1 \text{ km s}^{-1}$ <sup>5</sup>. Two of the published frames show maser peaks within 50 mas to the south and southwest of the star with velocities of  $29.8$  and  $37.8 \text{ km s}^{-1}$ , which may be coincident with inner the knot. For a direct comparison, we show the distribution of the maser emission at  $30.5 \text{ km s}^{-1}$  with the  $0''.1$  slit and the position of the inner knot superposed in Figure 3.

In an earlier study covering the entire envelope of VY CMa, Ziurys et al. (2007) concluded that the molecular maser and thermal emission and the K I emission traced the same outflows. We therefore suggest that the optical K I emission inner knot may coincide with the  $\text{H}_2\text{O}$  masers at similar velocities.

#### 4. The Knots and Clumps South and Southwest of the Star

Figure 4 shows a close-up of the positions of the three south (S) slits superposed on the F656N image. After acquisition, with the slit rotated to a position angle of  $125^\circ$ , the star was centered on the slit using a peak up in the red and an exposure taken.

The telescope was then offset to the positions shown in Figure 4,  $-0''.716$ (S1),  $-1''.088$ (S2), and  $-1''.425$ (S3). The two-dimensional spectrum of the K I lines in the three slits is shown in Figure 5 and the profiles corresponding to the K I emission peaks are shown in Figure 6. The same 5 pixel wide extractions along the slit were used for all of the spectra. The emission peaks were cross-identified with the diffuse knots and condensations visible in the image by comparing their measured positions along the slit with the positions of the emission peaks knowing the scale of the spectra and images. The identified knots are labeled in Figure 6 and are listed in Table 2. We follow the naming convention adopted in Humphreys et al. (2007), but note

<sup>5</sup> The correction to the LSR depends on the adopted solar motion. We use the solar motion from Schonrich et al. (2010). LSRK (local standard of rest (kinematic) used for the radio observations is based on the average velocity of stars near the Sun.

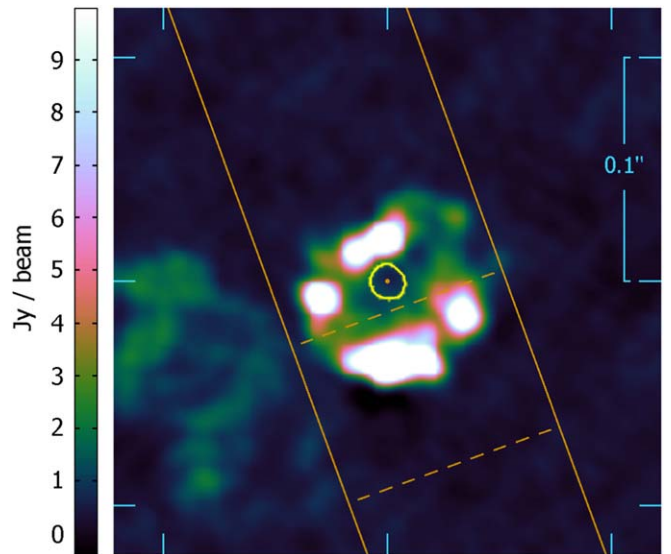


**Figure 3.** The  $\text{H}_2\text{O}$  658 GHz maser emission peaks within 100 mas of the star. The color scale is the 658 GHz maser in a  $2.2 \text{ km s}^{-1}$  (averaged) channel at  $30.5 \text{ km s}^{-1}$ , with the channel peak at  $34.72 \text{ Jy/beam}$  and a resolution of  $(10 \times 9)$  mas. The yellow contour encloses 50% of the continuum emission at 669 GHz; the dot marks the 99% contour of the  $107 \text{ mJy/beam}$  peak taken as the position of the star, at 7h 22 m 58.326 s,  $-25\text{deg } 46' 3''.04$ . The parallel orange lines map the position of the HST/STIS  $0''.1$  wide slit with a position angle of  $20^\circ$ . The two dashed lines bracket the 3 row/pixel extraction width for the spectrum of the K I emission feature that was centered at  $0''.05$  from the star. The 658 GHz image was provided by A.M.S. Richards, see Asaki et al. (2020).

that some of the features listed here were not included in that paper. They are identified as new measurements in the footnotes. In a couple of cases there is no obvious identification with a knot.

The profiles in Figure 6 illustrate the shift in the K I Doppler velocities of the knots along the slits relative to the K I velocity of the star shown as a dashed line. Unlike the complex profiles in Humphreys et al. (2005), these profiles with the narrow slit and extracted on specific knots are mostly symmetric and with a single velocity peak. The 2005 study used a much wider  $1''.0$  slit which intercepted multiple features especially crossing the arcs in the outer ejecta. The only profile that shows evidence of multiple peaks is S3 row 525, but there is no obvious identification with a condensation. Close inspection of S3 in Figure 5 shows a blueward extension on the K I emission at that row. The relatively bright extended nebulous feature, W1 knot C, contributes to both slits W1 and S1. The profile in Figure 6 is from S1, but spectra were extracted from both slits and their measurements are included in Table 2.

The measured Doppler velocities of the two K I emission lines are given in Table 2 with the velocity of the K I absorption feature, if present, and the average velocity of the absorption lines, with the number of lines in parenthesis, from the spectrum with grating tilt 8561. The radial velocity is the average velocity of the K I lines relative to the velocity of the K I lines in the star's spectrum measured in the  $0''.1$  slit (Table 1).

We determine the transverse velocity from the proper motions of the knots measured in the two epochs of HST/WFPC2 images from 1999 and 2005 as described in Humphreys et al. (2007). VY CMa was imaged in four filters, F410M, F547M, F656N, and F1042M, with a range of exposure times. The images are tightly aligned in pixel space and blinked to identify any offset. We measure the  $x$  and  $y$  positions of the blinked images three times in

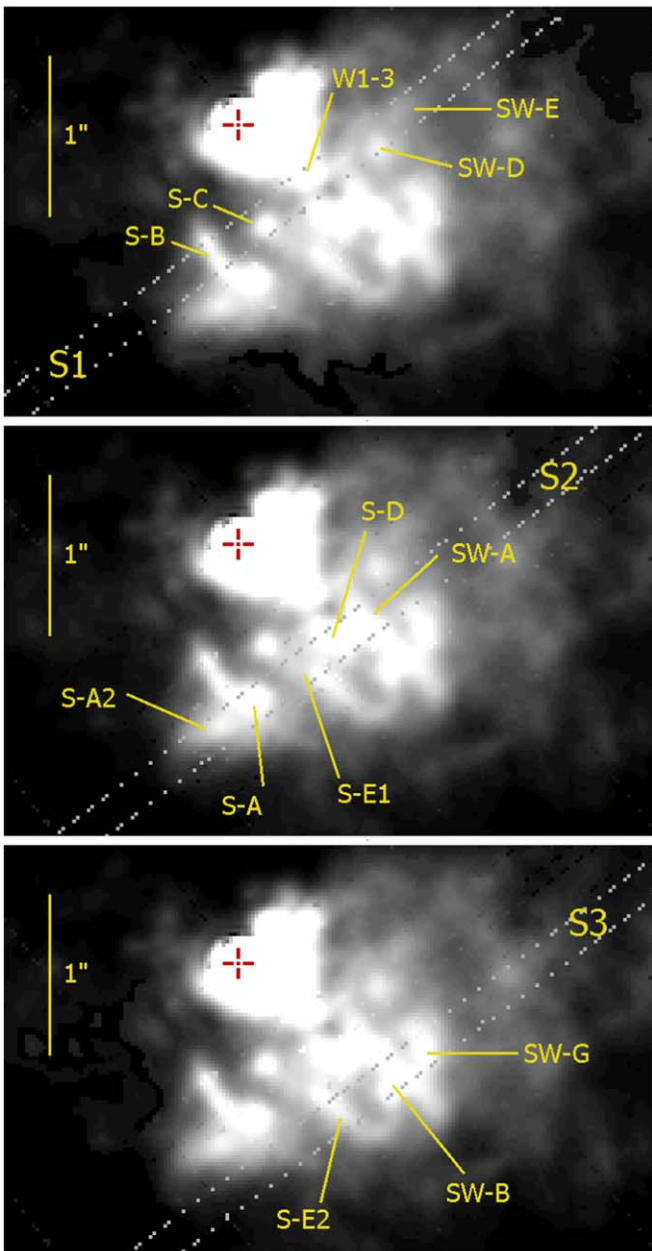


**Figure 4.** Locations of the three S slits on the red F656N image. The separate knots discussed here and listed in Table 2 are identified. The central star is marked by a red cross.

each filter combination in which the knot or filament is identified. The measurements are then combined for a weighted mean.

For this paper we checked all of our previous measurements, and in some cases repeated them to resolve discrepancies or multiple entries from the different filters. These are also noted in the footnotes. In all cases, the previous measurements were adjusted to the distance change from 1.5 kpc used in Humphreys et al. (2007) to 1.2 kpc (Zhang et al. 2012) and the change in the adopted velocity for the central star,  $55 \text{ km s}^{-1}$ ; see Paper I.

Combining the resulting transverse velocity with the radial velocity from the KI lines relative to the star, we then determine each knot’s orientation ( $\theta$ ) with respect to the plane of the sky, the direction of motion ( $\phi$ ), and total space velocity and then estimate its age or time since ejection assuming a

constant velocity. Although the winds of evolved cool stars are known to accelerate, these knots and arcs are discrete ejections, and it is not known if the plasma is accelerated or slowed by interaction with surrounding material.

(Acceleration and/or deceleration of the knots obviously affect these constant-velocity estimates. With credible parameters, however, the estimated times since ejection are altered by only a few percent. For instance, consider two simple models with an escape speed between  $55$  and  $90 \text{ km s}^{-1}$  just above the stellar surface, at  $r \approx 8 \text{ au}$ .<sup>6</sup> In one model, suppose that the ejecta were accelerated instantaneously in that region, and later were gravitationally decelerated as they moved outward. At radial distances of  $300$ – $800 \text{ au}$ , the true age since ejection is then about 10% smaller than the time estimated by our simplified constant-velocity estimate. Alternatively, suppose that the ejection process was quite gradual, with a net outward acceleration proportional to  $1/r^2$ . In that case, the true age is about 5% longer than the constant-velocity estimate. Further details are beyond the scope of this paper, but most likely ejection scenarios would produce results intermediate between these two cases.)

We note that most of these knots or features relatively near the star have approximately the same total velocity,  $\sim 20$ – $30 \text{ km s}^{-1}$ , and to a first order their age or time since ejection is correlated with distance from the star, which is not surprising. Based on their orientations and directions of motion the condensations to the southeast along S1 and S2 (S knots B, C, A, and A2) initially look as though they may be physically associated and from the same ejection event. However, they were apparently ejected at different times with ages that correlate with three active periods about 120, 200, and  $\approx 250 \text{ yr}$  ago, also indicative for several of the other knots and condensations.

In contrast, the knots to the south and west along S2 and S3 appear to be clustered around what looks like a darker patch or more correctly a region with low emission. These condensations are identified with an infrared bright feature called the SW clump (Shenoy et al. 2013; Gordon et al. 2019) and the knots were referred to as the SW knots in Humphreys et al. (2007).

#### 4.1. The SW Clump

The infrared bright feature visible in the longer wavelength images from  $1$  to  $10 \mu\text{m}$  to the southwest of the star is referred to as the SW clump in several papers (Humphreys et al. 2007; Shenoy et al. 2013; Gordon et al. 2019). Several knots and diffuse condensations identified with this feature in Table 2 appear to be spatially distributed around a region of lower flux that appears dark in the visual images. Figure 7 shows the HST  $1 \mu\text{m}$  image with the  $Ks$  ( $2.15 \mu\text{m}$ ) image from the Large Binocular Telescope (LBT)/L/M-band InfraRed camera (LMIRcam) reproduced from Shenoy et al. (2013). The visual knots are marked on the  $1 \mu\text{m}$  images and possible cross-identifications are shown on the  $Ks$  image. Note that the  $2 \mu\text{m}$  image shows the same basic structure as the  $1 \mu\text{m}$  picture with knots distributed in a rather elongated shape around a region of lower emission. Comparison of the superposed HST visual and  $1 \mu\text{m}$  images suggests that most of the near-infrared flux

<sup>6</sup> The escape velocity depends on the mass of the star. Based on its luminosity, VY CMa had an initial mass of  $\sim 30 M_{\odot}$ , possibly as high as  $35$ – $40$ . It has had a very high mass-loss rate as an red supergiant and substantial mass loss on the main sequence. It therefore may have shed half its mass. Assuming a current  $20 M_{\odot}$  gives  $70 \text{ km s}^{-1}$  for the escape speed.

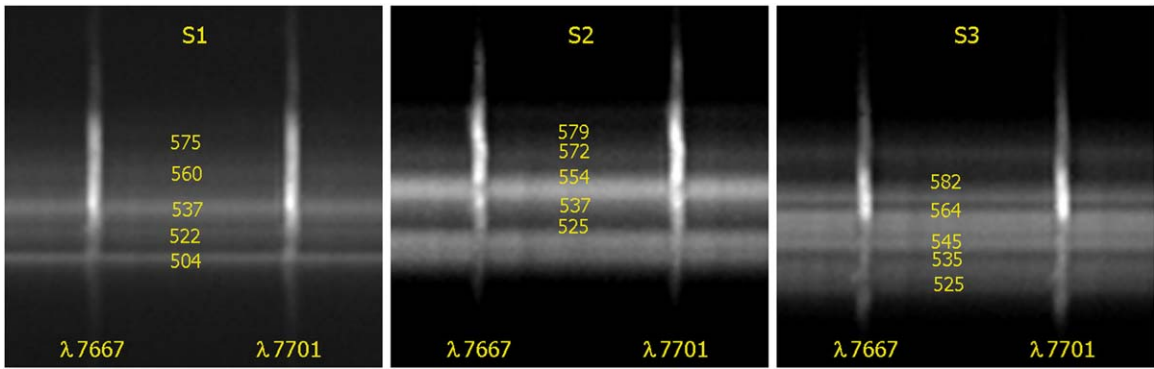


**Figure 5.** The two-dimensional images along the three slits showing the K I emission perpendicular to the dispersion with the row numbers in pixels corresponding to the profiles in Figure 6.

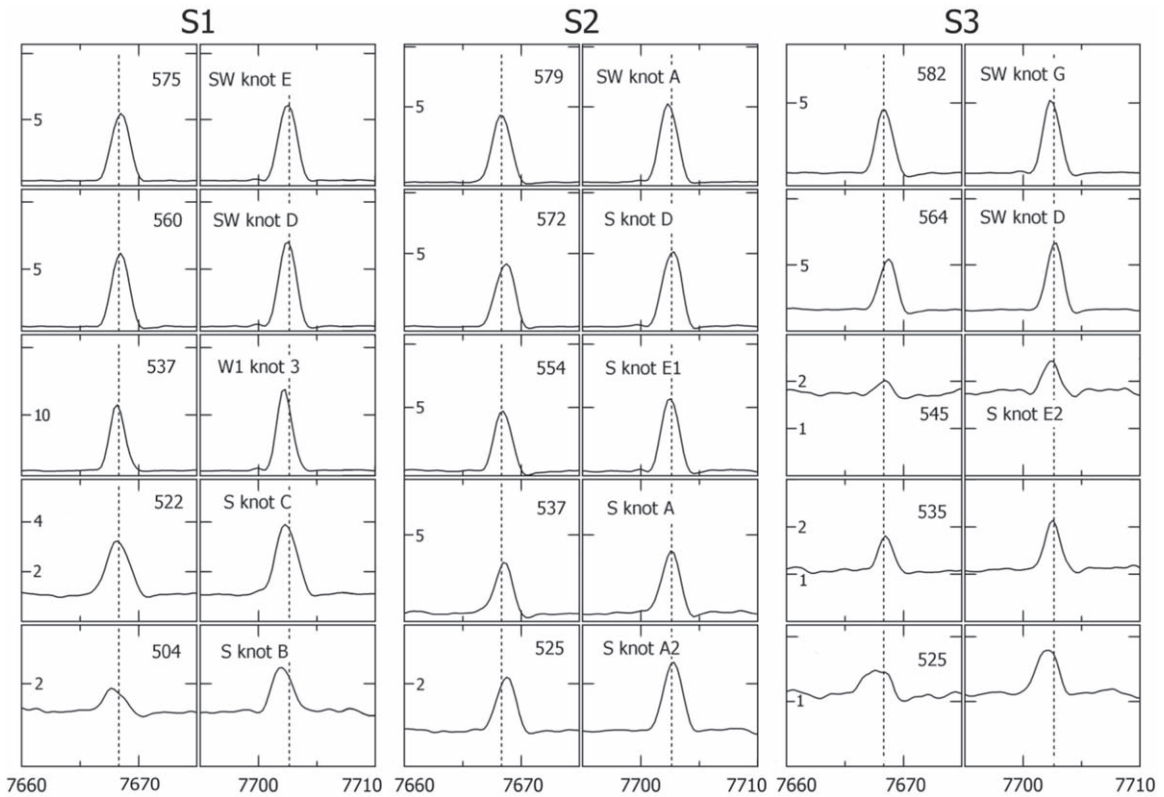


**Figure 6.** The K I emission line profiles extracted along the slits. The row number (Figure 5) is given in the panel for the  $\lambda 7667$  line and the knot identification in the neighboring profile for the  $\lambda 7701$  line. The flux calibrated spectra are in units of  $10^{-14}$  W  $\text{cm}^{-2}$  vs. the vacuum wavelength in  $\text{\AA}$ .

appears to be coming from S knot D and SW knot A, which are also the two largest knots and are the closest to the star. Thus separate knots may contribute to the strong infrared flux identified as the SW clump.

The four or five knots identified in the visual image (Figure 4) appear to be distributed in an arc or possible elliptical shape around the dark, lower density region. This is suggestive of an expanding large knot or bubble with the knots on the outer rim. The apparent nonradial motion (with respect to the star) specifically of S knot E2 and SW knot B support a possible expanding bubble. This reminds us of the nearly circular arcs in the inner ejecta of the warm hypergiant IRC +10420 that were shown to be expanding bubbles (Tiffany et al. 2010).

To test this possibility, we fit an ellipse to the positions of the knots in the two epochs, 6.23 years apart. Comparing these

loops or arcs via cross-correlations would be difficult because their inner knots are much brighter than their outer parts. Faint S knot E1 was excluded because its position is relatively uncertain. Thus, in order to have five points necessary to define an ellipse, we used a point on the south rim, part of a luminous arc on the apparent south side of the SW clump. Its position is less well defined than the other knots and it has no velocity measurement. Obviously it would be better to use more than five spatial points, but no other features were suitable. Since the intrinsic deviations from a true ellipse are presumably similar for both epochs, we can meaningfully compare these two ellipses.

The best-fit ellipse is shown superposed on the F656N image from 1999 in Figure 8. The parameters from the ellipse fits are summarized in Table 3. The two ellipses coincide with an rms difference of 16 mas when we allow for expansion, and the

**Table 2**  
Summary of Measured Heliocentric Velocities, Motions, and Ages

Object Name	K I Em. Velocity (km s <sup>-1</sup> )	K I Abs Velocity (km s <sup>-1</sup> )	Abs. Line Velocity (km s <sup>-1</sup> )	Radial Velocity (km s <sup>-1</sup> )	Trans. Velocity (km s <sup>-1</sup> )	Total Velocity (km s <sup>-1</sup> )	Direct. $\phi$ (deg)	Orient. $\theta$ (deg)	Dist. (au)	Age (yr)	Comment
S knot B	25.4, 30.0	...	-43.6	75.0 ± 9.9 (16)	-26.8 ± 1.4	30.2 ± 2.5	40.4 ± 2.8	148 ± 7	-41.6 ± 3	1020	Slit S1
S knot C	41.5, 43.6	...	...	68.8 ± 9.4 (15)	-12.2 ± 2.2	18.2 ± 1.0	21.8 ± 2.4	151 ± 12	-33.8 ± 8	876	Slit S1
W1 knot C <sup>b</sup>	42.2, 41.6	...	-22.5	79.9 ± 9.1 (17)	-13.5 ± 3.2	21.9 ± 2.7	25.7 ± 4.2	-134 ± 4	-31.6 ± 9	636	Slit S1
...	46.1, 44.8	-12.1, -18.3	...	72.9 ± 8.4 (15)	-8.6 ± 4.0	...	23.5 ± 5.0	...	-21.4 ± 10	...	Slit W1
SW knot D	55.2, 53.0	...	-21.4	95.9 ± 11.0 (15)	-1 ± 3.8	23.5 ± 3	23.5 ± 4.8	-63 ± 11	-2.4 ± 10	993	Slit S1
SW knot E	55.2, 53.7	...	...	86.1 ± 13.9 (13)	-0.5 ± 2	15.6 ± 4.5	15.6 ± 5	-116 ± 10	-1.8 ± 10	1260	Slit S1
S knot A <sup>2c</sup>	68, 64	...	...	90.5 ± 8.6 (16)	11 ± 4.2	25.2 ± 5.5	27.5 ± 7	135 ± 12	21.8 ± 10	1380	Slit S2
S knot A	58.7, 58.4	...	...	94.3 ± 8.0 (15)	4.4 ± 2.6	29.4 ± 2.4	29.7 ± 5	177 ± 5	8.5 ± 8	1170	Slit S2
S knot E1 <sup>d</sup>	52.8, 53.3	...	-20	96.9 ± 10.1 (15)	-2.0 ± 4.2	20.1 ± 7.2	20.2 ± 7.4	77 ± 16	-5.6 ± 16	1156	Slit S2, SW clump
S knot D <sup>e</sup>	65.7, 64.6	...	-23.4	88.1 ± 13 (13)	10.2 ± 5	17.1 ± 4.7	19.9 ± 6.9	-120 ± 8	27 ± 10	1016	Slit S2, SW clump
SW knot A	48.9, 47.1	...	-28	94.9 ± 8.5 (14)	-7.0 ± 5	24.1 ± 2.5	25.1 ± 5.5	-101 ± 23	-16.2 ± 10	1200	Slit S2, SW clump
S knot E2 <sup>d</sup>	54.0, 52.5	...	-18.7	84.5 ± 8.7 (16)	-1.75 ± 3.5	19.1 ± 3.5	19.2 ± 5	146 ± 5	-5.2 ± 10	1380	Slit S3, SW clump
SW knot B <sup>f</sup>	64.2, 62.7	...	...	95.2 ± 11.0 (16)	8.5 ± 5	21.5 ± 5	23 ± 7	-47 ± 10	21.6 ± 10	1460	Slit S3, SW clump
SW knot G <sup>g</sup>	50.0, 48.3	...	-22.2	93.1 ± 9.2 (16)	-5.9 ± 2.5	26.5 ± 3	27.1 ± 4	-143 ± 4	-12.5 ± 6	1490	Slit S3

**Notes.**

<sup>a</sup> The average K I em velocity relative to the K I emission line velocities measured on the star with the 0<sup>0</sup>/1 slit. See Table 1 and Paper I.

<sup>b</sup> This condensation is measured in slits S1 and W1.

<sup>c</sup> New measurement, not included in Humphreys et al. (2007).

<sup>d</sup> S knots E1 and E2. This feature was measured but not included in Humphreys et al. (2007). The faint extension, E1, on slit S1 and the brighter, E2, in S3 were measured separately. The large uncertainties on E1 are due to its faintness.

<sup>e</sup> Two features D1 and D2 were identified in Humphreys et al. (2007) with discrepant measurements in different filters. Remeasured.

<sup>f</sup> Remeasured.

<sup>g</sup> Discrepant measurements in Humphreys et al. (2007). Remeasured.

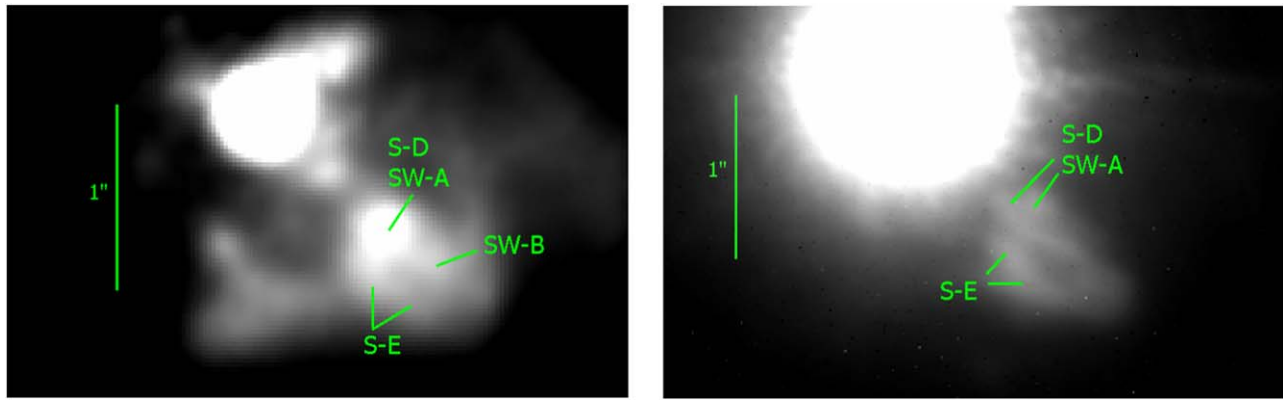


**Figure 7.** Left: the HST F1042 image with the positions of the visual knots identified. Knots S-D and SW-A are merged in the  $1\ \mu\text{m}$  image. Right: the  $K_s$  band images from Shenoy et al. (2013). Possible cross-identifications of the partially resolved features from the visual images are marked.

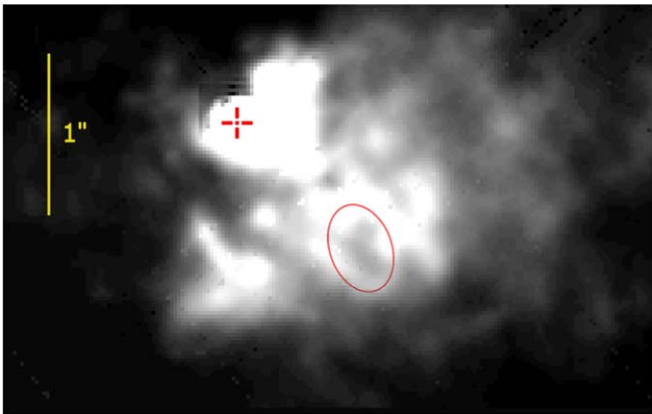


**Figure 8.** Ellipse fit to the knots possibly associated with the SW clump shown superposed on the 1999 red F656N image.

**Table 3**  
Ellipse Fits

Epoch	Major Axis (au)	Major Axis PA	Center Dist. (au)	Center PA
1999.22	$0''.562$ (675)	+20 deg	$1''.090$ (1310)	+44 deg
2005.45	$0''.575$ (691)	+12 deg	$1''.123$ (1350)	+43 deg

disagreement in the radial direction is of the order of 5 mas; this is satisfactory considering the fuzziness of each data point.

The centers of the two ellipses are consistent with an expansion age of about 200 years relative to 1999 (projected velocity  $\sim 25\ \text{km s}^{-1}$ ), while the major-axis expansion similarly indicates about 260 yr. These values are comparable with other features south and southwest of the star. Although the visual images and the ellipse fits are encouraging, there are problems with this model for S knot D and SW knot A. Both have a direction of motion consistent with radial motion outward from the star as opposed to an expanding outer shell of a bubble moving away from the ellipse center. The positive radial velocity for S knot D shows it is projected backward, away from the plane of the sky, while SW knot A is forward, in front of the plane of the sky.

An alternative possibility would place S knot E2 and SW knot B and the south rim on an expanding arc or loop like several small arcs seen throughout the ejecta as well as the giant arcs/loops in the outer ejecta. SW knot B is projected away from us but its orientation is consistent with the far side

of a loop tilted with respect to our line of sight. If that is the case, this arc or loop would have been ejected about 300 years ago, and S knot D and SW knot A would then be chance superpositions from later eruptions.

Thus it is not clear if the SW clump is a coherent object, or chance alignment of unrelated clumps of dust and gas. The  $2\text{--}5\ \mu\text{m}$  imaging by Shenoy et al. (2013) still puts strong constraints on the feature. The high surface brightness requires that the illuminated clump(s) have a relatively clear line of sight to the star and be optically thick to scattering by dust. The imaging polarimetry (Shenoy et al. 2015) constrains the albedo to 40% or less, otherwise multiple scattering would reduce the observed fractional polarization at  $3.1\ \mu\text{m}$  below the observed value. These observations combined with the optically thick emission observed at  $11\ \mu\text{m}$  (Gordon et al. 2019) require that a minimum mass of  $5 \times 10^{-3} M_{\odot}$  must be present in the knots, whether they are kinematically related or not.

Another example is shown in a recent paper on high-resolution imaging with ALMA (Asaki et al. 2020). Images at  $\sim 10\ \text{au}$  (8 mas) resolution show that ALMA clump C in VY CMa is resolved into many small condensations of higher and lower intensity making up the total flux density detected at lower resolution. The condensations have a range of apparent sizes, but most appear to be much smaller than the knots in the visual and near-infrared images discussed here, although clump C is much younger than the SW clump (see Section 5) and may expand with time.

## 5. The Mass-loss History

The most important conclusions from our previous studies of VY CMa (Humphreys et al. 2005, 2007; Jones et al. 2007) were not only the very visible evidence for high mass-loss episodes, but the massive outflows in different directions ejected at different times over several hundred years, suggestive of significant periods of surface activity. With the improved spatial resolution from the STIS spectra, we have determined the ejection ages for the separate knots within about 1 arcsecond of the star. The closest, along slits W1, W2, and E, were apparently ejected within the past century (Paper I), and the inner knot described in this paper was ejected  $\approx 1985\text{--}1990$ . The numerous knots to the south and southwest, including those associated with the SW clump, have ejection ages which concentrate around 120, 200, and 250 years ago.

For comparison with the large arcs and features visible in the more distant ejecta (Humphreys et al. 2007), we have redetermined their ejection ages (Table 4) with the improved distance to VY

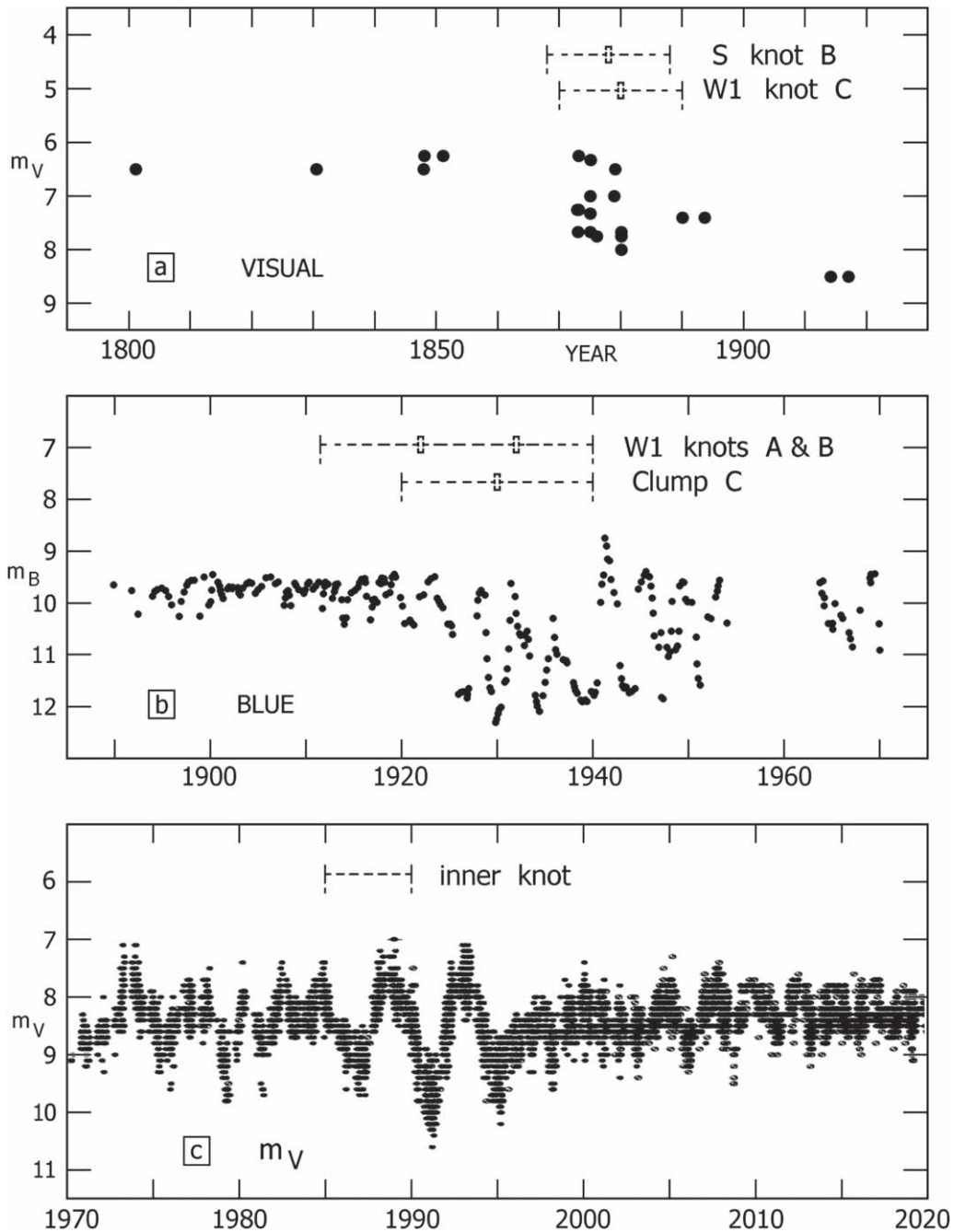


**Figure 9.** The light curves with the probable ejection times for the different knots. Upper panel (a): the light curve for the 19th century (Robinson 1971). Middle panel (b): mid-20th century (Robinson 1970). Bottom panel (c): the most recent photometry from the AAVSO. We use the ages based on an assumed constant velocity. Uncertainty due to acceleration or deceleration is small (Section 4), comparable to the error bars from other sources.

CMa (Zhang et al. 2012) and our radial velocity for the central star from Paper I (see Table 1). The revised ages average slightly less than reported in our 2007 paper. Our mid- and far-infrared observation with the Stratospheric Observatory for Infrared Astronomy (SOFIA; Shenoy et al. 2013) found no extended cold dust with an age greater than about 1200 years. Combined with our current measurements, VY CMa thus has a history of discrete mass-loss events over the past 1000 years which appears to be continuing.

In Figure 9, we show the light curve of VY CMa from 1800 to 2000. The upper panel for the 19th century is from the table

**Table 4**  
Revised Ejection Ages for Major Features

Feature	Ejection Age (yr)
Northwest arc	534
Arc 1	637
Arc 2	400
West arc	312
South arc	373
SE loop	271
Outer spikes	1000–1500

in Robinson (1971). We use the magnitudes from his column four which are reduced to the Harvard photometry and are approximately visual magnitudes. The second panel is from Robinson (1970) and are blue magnitudes measured from the Harvard patrol plates<sup>7</sup> from about 1900 to 1950. The points from  $\sim 1963$  to 1970 are from the Remeis Observatory, see Robinson (1970). The bottom panel shows the more recent visual magnitudes from the American Association of Variable Star Observers (AAVSO).

Several features are notable. VY CMa was nearly visible by the naked eye at about 6–6.5 mag at the start of the 19th century until a major period of variability from  $\approx 1870$  to 1880 with multiple dimmings. There is a 20 year gap from  $\sim 1850$  to 1870, but by 1872 the star is a magnitude fainter. There are three recognizable minima. The decline to about 8 mag in 1880 is followed by a gap of 10 years. We do not know if the star recovered or had additional minima, but by 1890–1893, it was a magnitude below its unobscured brightness. Fortunately the 20th century light curve, (middle panel) overlaps the 1890–1910 period with no additional deep minima and confirms the decline by 1–1.5 mag to 7.5–8 mag in the visual (9.5–10 blue mag). It has stayed near this fainter magnitude since. Today VY CMa is typically 8 mag in the visual with a  $B-V$  color of  $\approx 2.0$ . Since the 19th century the light curves show two periods with significant variability, from  $\approx 1925$  to 1945, with dimming by two or more magnitudes in the blue and more recently from about 1985 to 1995 dimming by 1–1.5 mag in the visual.

The ejection ages of several of the knots are marked on the light curves. We emphasize that they agree with these extended periods of variability and change. The most recent, the inner knot visible in the narrow slit on the star, is consistent with an ejection during VY CMa’s most recent active period. The knots discussed in Paper I, along slit W1, have ejection dates from  $\approx 1920$  to 1940 corresponding to the long very active period.

In a recent paper on the dusty obscured clumps discovered with ALMA, Kaminski (2019) discussed the masses, ages, and other properties of the condensations in this prominent feature just to the east of the star. Kaminski also compared his estimated ages with the 20th century light curves shown here in Figure 9. Unlike our results, he concluded that there was no correlation between their ages and the extended periods of variability. However, he adopted a rather high expansion velocity of  $60 \text{ km s}^{-1}$  for the clumps. Velocities this high are only measured for a couple of the most distant arcs (Humphreys et al. 2007). The average outflow velocity for the small knots close to the star (Paper I) and at comparable projected distances as the ALMA clumps is  $27.5 \text{ km s}^{-1}$ . With this adopted velocity we estimate an age of about 70 years for clump C, corresponding with the extended period of large light variations in the first half of the 20th century (Figure 9).

The most interesting period may be 1870–1880 and the post-1880 fading from which VY CMa has not recovered. S knot B and W1 knot C plus possibly the W2 knot have ejection ages that correspond to this period. Their different locations and orientations with respect to the star suggest that surface activity occurred over much of the star with separate outflows in different directions lasting at least 10 years. The major dimming of the star after 1880 by one or more magnitudes is very likely the origin of the present obscuration of the central star, the VY peak in the ALMA images. One of the unexpected

conclusions in Paper I was the requirement that the visible compact knots just to the west of the star have a relatively clear line of sight to the star to explain their very strong KI and molecular emission. We thus suggested that there must be a hole or gaps in the surrounding circumstellar ejecta near the star. Alternatively, the very dusty VY may not completely surround the star and is not obscuring it in all directions, but is instead a large knot, possibly similar to clump C in the ALMA maps, ejected in  $\sim 1880$  nearly in our line of sight. This possibility also helps explain the strong KI lines observed in some of the knots to the south of the star suggesting a clearer line of sight to the star in other directions as well.

### 5.1. Comments on Betelgeuse

The famous red supergiant visible by the naked eye Betelgeuse ( $\alpha$  Ori) recently experienced an unexpected visual dimming beginning in 2019 December and continuing well into 2020 (Guinan et al. 2019, 2020) reaching an unprecedented minimum in 2020 February, fading by about 1 mag. A visual image from 2019 December observed with the Spectro-Polarimetric High-contrast Exoplanet REsearch instrument (SPHERE) on the Very Large Telescope (VLT) showed a remarkable corresponding fading of its southern hemisphere (M. Montargès 2020, in preparation). At about the same time UV spectra from HST/STIS revealed remarkable changes with an increase in the UV flux and variations in the Mg II line supporting a corresponding outflow of material from the star (Dupree et al. 2020). The dimming in the light curve is attributed to dust, although other authors have questioned this (Harper et al. 2011; Dharmawardena et al. 2020), and suggest that a change in the photospheric luminosity or a cooling of a large fraction of the photosphere due to dynamical effects may be responsible.

The similarity of the correspondence between the periods of variability and dimming in VY CMa and in Betelgeuse with outflows of gas is clear. Furthermore, high-spatial near- and mid-infrared imaging of Betelgeuse (Kervella et al. 2009, 2011) reveals several clumps or knots of dusty material within 1 arcsecond of the star. This current ejection by Betelgeuse may be similar to the recent inner knot ejection observed in VY CMa’s spectrum or to its 1920–1940 active period, depending on how long its current variability lasts.

With its very extended and complex ejecta, the much more luminous and more massive VY CMa is clearly a more extreme example of a high mass-loss event extending over several hundred years. There is definitely a difference in scale and very likely in the energies involved. For example, the deep minima in VY CMa typically lasted about 3 years, and longer in a couple of cases, while the dimming in Betelgeuse only lasted about 150 days. Nevertheless, the presence of outflows from the surface of the more typical red supergiant Betelgeuse suggests that these discrete mass-loss episodes are not unique to the extreme hypergiants like VY CMa and IRC +10420 (Tiffany et al. 2010). The evidence for similar activity in other red supergiants should be more fully explored. The strong maser sources are obvious candidates (Schuster et al. 2006; Humphreys et al. 2020), and clumpy winds have been reported for  $\alpha$  Sco (Ohnaka 2014) and  $\mu$  Cep (Montargès et al. 2019). Surface activity and the accompanying outflows may thus be a major contributor to mass loss in these red supergiants.

<sup>7</sup> VY CMa is not yet in the online database for the DASCH digitization of the Harvard plate collection.

### 5.2. Outflows and Ejections: Pulsation and/or Surface Activity?

Betelgeuse is a known semi-regular variable with a period of  $\approx 400^d$  attributed to radial pulsations plus a longer  $\approx 2000^d$  period associated with convective/magnetic activity. Betelgeuse is also well known for large, bright regions associated with convective cells. Dupree et al. (2020) suggest that the outflow in Betelgeuse from a convective cell was enhanced by the outward motion in its  $400^d$  radial pulsation. The outflow expanded and cooled obscuring the southern hemisphere and possibly forming dust causing the deep dimming in its visual light curve.

The light curve of VY CMa provides a somewhat different perspective with a complex history of extended periods of activity or dimming lasting 10–20 years separated by long periods of relative quiescence. VY CMa is not known to show radial pulsations. It is an irregular variable.

We find probable correlations of two to three separate mass ejections or outflows with the 19th century episode and with the 1920–1940 period suggesting that each of the minima may be related to a separate outflow. If the deep minima, which last 3 years or more, are caused by dust formation, their longer duration suggest that the ejections are more massive, perhaps implying more dust and obscure the star for longer. Except for post-1880–1890, in each case, VY CMa returned to its previous brightness. Our measurements show that the knots are moving in different directions with different spatial orientations, and thus will eventually move out of our line of sight. We have suggested here that the major and continued dimming after 1880, is due to a dusty outflow nearly in our line of sight.

Based on the light curve of VY CMa, a recurring radial pulsation period seems an unlikely cause or enhancer for its multiple outflows and minima. In our previous papers on VY CMa and other evolved supergiants with high mass-loss episodes such as IRC 10420, we have attributed the separate outflows and ejections to large-scale surface and magnetic activity. By analogy with Betelgeuse, we expect that VY CMa will have extensive surface asymmetries, large convective cells, or regions covering much of its surface, which could be responsible not only for major outflows but for the equivalent of coronal mass ejections but on a larger scale. Nonradial pulsation is a possibility, but how would one separate that from large active regions on a star with a radius of  $\approx 7$  au?

This work was supported by NASA through grant GO-15076 (PI: R. Humphreys) from the Space Telescope Science Institute.

L. Ziurys acknowledges support from NSF grant AST-1907910. Based on ALMA data: ADS/JAO.ALMA#2011.0.00006.E.

Facilities: HST(STIS), AAVSO.

### ORCID iDs

Roberta M. Humphreys  <https://orcid.org/0000-0003-1720-9807>

A. M. S. Richards  <https://orcid.org/0000-0002-3880-2450>

Terry J. Jones  <https://orcid.org/0000-0002-8716-6980>

### References

- Asaki, Y., Maud, L. T., Fomalont, E. B., et al. 2020, *ApJS*, **247**, 23
- Davidson, K. 2006, in *The 2005 HST Calibration Workshop: Hubble After the Transition to Two-gyro Mode*, ed. A. M. Koekemoer, P. Goudfrooij, & L. L. Dressel (Baltimore, MD: STScI), 247
- Dharmawardena, T. E., Mairs, S., Scicluna, P., et al. 2020, *ApJL*, **897**, L9
- Dupree, A., Strassmeier, K. G., Matthews, L. D., et al. 2020, *ApJ*, **899**, 68
- Gordon, M. S., Jones, T. J., Humphreys, R. M., et al. 2019, *AJ*, **157**, 57G
- Guinan, E. F., Wasatonic, R. J., & Calderwood, T., Jr. 2019, *ATel*, **13341**, 1
- Guinan, E. F., Wasatonic, R. J., & Calderwood, T., Jr. 2020, *ATel*, **13341**, 1
- Harper, G. M., Guinan, E. F., Wasatonic, R., & Ryde, N. 2020, *ApJ*, **905**, 34
- Humphreys, R. M., Davidson, K., Ruch, G., & Wallerstein, G. 2005, *AJ*, **129**, 492
- Humphreys, R. M., Helmel, G., Jones, T. J., & Gordon, M. S. 2020, *AJ*, **160**, 145
- Humphreys, R. M., Helton, L. A., & Jones, T. J. 2007, *AJ*, **133**, 2716
- Humphreys, R. M., Ziurys, L. M., Bernal, J. J., et al. 2019, *ApJL*, **874**, L26
- Jones, T. J., Humphreys, R. M., Helton, L. A., Gui, C., & Huang, X. 2007, *AJ*, **133**, 2730
- Kaminski, Th 2019, *A&A*, **627**, 114
- Kervella, P., Perrin, G., Chiavassa, A., et al. 2011, *A&A*, **531**, A117
- Kervella, P., Verhoelst, T., Ridgway, S. T., et al. 2009, *A&A*, **504**, 115
- Montargès, M., Homan, W., Keller, D., et al. 2019, *MNRAS*, **485**, 2417
- O’Gorman, E., Vlemmings, W., Richards, A. M. S., et al. 2015, *A&A*, **573**, L1
- Ohnaka, K. 2014, *A&A*, **568**, A17
- Robinson, L. 1970, *IBVS*, **465**, 1
- Robinson, L. 1971, *IBVS*, **599**, 1
- Schonrich, R., Binney, J., & Dehnen, W. 2010, *MNRAS*, **403**, 1829
- Schuster, M. T., Humphreys, R. M., & Marengo, M. 2006, *AJ*, **131**, 603
- Shenoy, D., Jones, T. J., Humphreys, R. M., et al. 2013, *AJ*, **146**, 90
- Shenoy, D., Jones, T. J., Packham, C., & Lopez-Rodriguez, E. 2015, *AJ*, **150**, 15
- Tiffany, C., Humphreys, R. M., Jones, T. J., & Davidson, K. 2010, *AJ*, **140**, 339
- Vlemmings, W. H. T., Khouri, T., Marti-Vidal, I., et al. 2017, *A&A*, **603**, 92
- Zhang, B., Reid, M. J., Menten, K. M., & Zheng, X. W. 2012, *ApJ*, **744**, 23
- Ziurys, L. M., Milam, S. N., Aponi, A. J., & Woolf, N. J. 2007, *Natur*, **447**, 1094